XX IMEKO World Congress
Metrology for Green Growth
September 9–14, 2012, Busan, Republic of Korea

MEASUREMENT OF EFFECTIVE ELECTRON SOURCE SIZE BY USING NANO-BIPRISM

B. Cho/Presenter, Y. Cho, S. Ahn, H. Lee, B. Park and C. Hwang

Korea Research Institute of Standards and Science, 267 Gajeong-ro, Yuseong-gu, Daejeon 305-340 Rep. of Korea, blcho@kriss.re.kr

Abstract: The spatial coherence length of electron beam was measured by using multi-walled carbon nanotubes as an element of a nano-biprism. With decreasing the source temperature from 300K to 78K, the visibility of the interference fringe of emitted electrons increases by a factor of 3, and the band of the interference pattern widens by a factor of 5.

Keywords: coherence length, electron beam, biprism.

1. INTRODUCTION

Field emission (FE) electron source has been a main driving force of modern high-resolution electron microscopy and interferometry because of its high brightness [1]. It has small spatial size of ~50 nm and narrow energy width of 0.3 eV; the former directly relates to spatial coherence and the latter to temporal coherence.

The coherence of an electron beam (e-beam) can be evaluated if there are interference or diffraction fringe patterns produced by it [2]. According to the coherence theory, the visibility of the fringe patterns improves with the enhancement of the degree of coherence of the e-beam [3]. In this regard, projection microscopy (PM) is a useful tool for the coherence evaluation of electron beam because it is one of the simplest methods to present electron interference patterns. Actually the transverse coherence lengths of various field emitters have been measured using Fresnel edge fringe patterns in PM images [4-6]. However it is well known that the intensity of Fresnel edge fringes depends greatly on the edge shape and thickness [7].

Irradiated by electron beam, extremely narrow carbon fibers have been reported to work as a nano biprism [8]; electron biprism is a conventional tool for electron beam coherence test [2]. If such a nano biprism can be employed for coherence test, the measurement of coherence would be more reliable.

Here we show that the highly coherent electrons were emitted from a finite area. The coherence of the emitted electrons is related to the coherence of the original states of the emitter. With decreasing the source temperature from RT to 78K, the visibility of the interference fringe of emitted electrons increases by a factor of 3, and the band of the interference pattern widens by a factor of 5. Interference of highly coherent electrons generates multi electron beams which might be used in many kinds of instruments.

2. EXPERIMENTAL APPARATUS

A. General [9]

The ultrahigh vacuum (UHV) system is divided into a preparation chamber equipped with a simple field emission microscopy (FEM) system and main chamber housing low-temperature FE system. Figure 1 shows a schematic representation of the entire system. The loadlock, preparation chamber and the control electronics are based on a standard commercial design. The main chamber is connected to the preparation chamber though an all-metal gate valve. Both chambers are equipped with a sputter ion pump and a titanium sublimation pump. The base pressures in the preparation and main chamber are below 2×10^{-8} Pa and below 3.0×10^{-8} Pa without cooling, respectively. A load lock chamber is used to exchange tips and anodes in and out of the UHV environments without venting the entire system to atmosphere (venting the entire system, baking out, and returning to low temperatures require at least ten days turn-around time). The UHV chambers housing the entire system are isolated from floor vibrations by bolting them to an optical tabletop fitted with pneumatic legs.

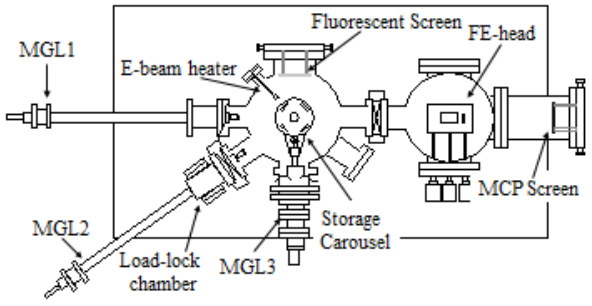

Figure 1. Schematic view of a low-temperature FE-system.

B. Preparation chamber

The preparation chamber is equipped with an e-beam heater and a storage carousel for storing two tip sockets and two anode holders. The e-beam heater is used for tip and anode cleaning. In order to preclude discharge at the apex of sharp tips during e-beam heating, the tantalum filament (0.2 mm) of the heater was shaped into a loop inside which

tips are placed by manipulating the carousel. The observation of FEM pattern is often necessary for evaluating the apex state of a tip. However the electron beam from a FE-tip should pass through three small holes at the radiation shields in the present low temperature FE-system and only a small portion of the beam can be projected on the screen outside the cooling system. To overcome this problem, a simple FEM system was installed inside the preparation chamber. The FEM system consists of a fluorescent screen and an extractor made of tantalum plate with holes (5mm). During and just after baking out, the screen and the extractor are fully degassed by e-beam bombardment using a tantalum filament installed on the backside of the extractor.

C. Low temperature FE-system

The extraction of monochromatic e-beam from a superconducting niobium tip requires the tip temperature to be lower than its critical temperature of 9.25 K with good margin. So the FE-head was mostly made of oxygen free highly conductive copper (OFHC) and directly bolted to the OFHC bottom of the central liquid helium tank in order to ensure good thermal conduction. A sheet of gold foil was laid between the FE-head and the bottom of the tank to enhance the surface contact. The cooling system is composed of three radiation shields, two liquid helium tanks and one liquid nitrogen tank made of stainless steel. The central and outer helium tanks have the capacities of 8 *l* and 5 *l*, respectively. The FE-head is housed inside three radiation shields made of gold plated OFHC. The inner one is bolted directly to the outer liquid helium tank, and the outermost one to the liquid nitrogen tank. In order to remove stray magnetic field effect on e-beams, the outside of the outermost radiation shield was lined with permaloy and all the parts of the FE-head were made of non-magnetic materials.

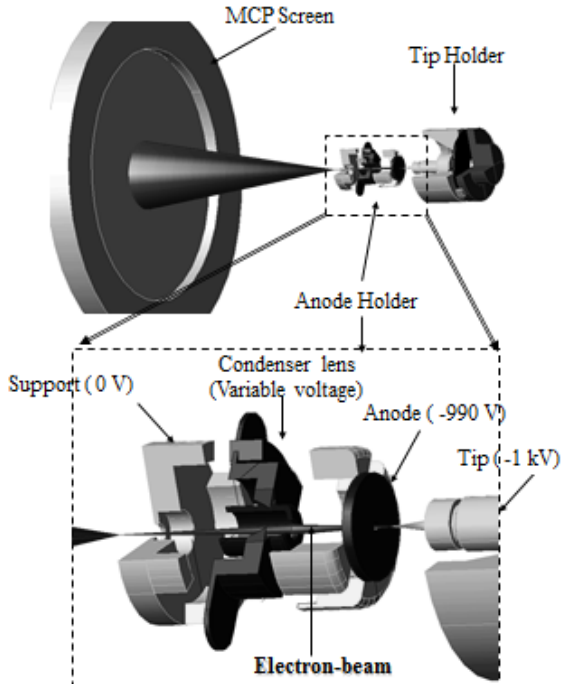

Figure 2. Scheme of the FE experiment. The electron beam extracted from a FE-tip is collimated by the condenser lens inside the anode holder and projected on the MCP. The enlarged view of the anode holder shows the condenser lens and the beam path inside the holder.

Except the anode holder, which has a simple condenser lens and a hole at the base (Fig. 2), the FE-head of the present system is based on conventional STM designs. As shown in the Fig. 3, a tip socket and anode holder are transferred from the preparation chamber to the FE-head using a magnetic transfer rod (MGL1) and loaded on the tip and anode stages, respectively, by snapping them into the

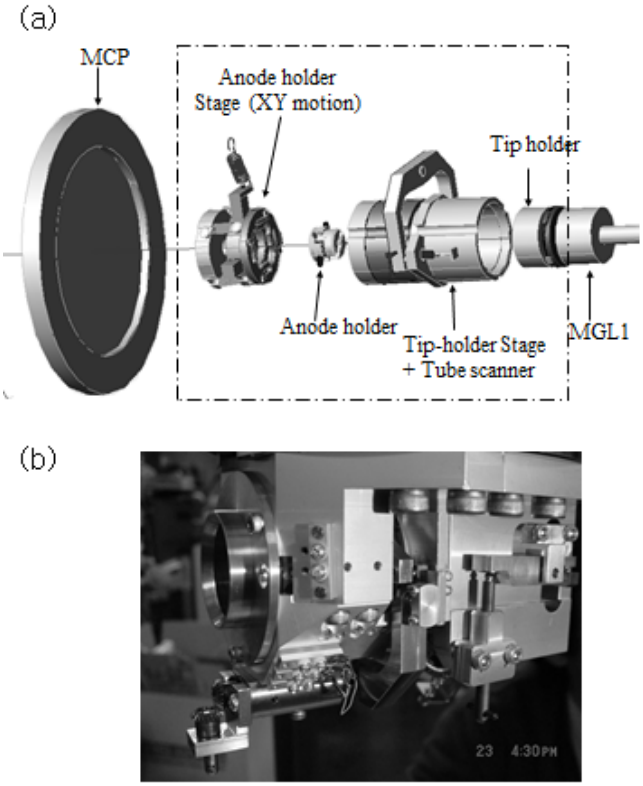

Figure 3. (a) View showing the key features of the FE-head. (b) Picture of the FE-head.

grooves of the stages. The anode holder is held to the anode stage with four beryllium-copper spring clips. The spring clips also serve as electrodes, providing four electrical connections to the anode holder. These four electrical connections will be used for functional expansion of the anode holder; insertion of electron bi-prism or einzel-lens inside the holder.

A piezotube is employed for the fine X, Y and Z movements of the tip. The coarse motions are conducted mechanically using levers, fine-pitch lead screws, bevel gears and rotary-motion feedthroughs driven by DC motors. For the X, Y coarse motions, the anode stage changes its position while the FE tip approaches the anode for the Z coarse motion. An OFHC copper case house the piezotube, tip stage and anode stage completely, enhancing the temperature stability of the tip and anode. Sapphire was used for electrical isolation wherever possible because of its

high thermal conductivity at low temperature. The electrical connections to the FE-head are heat sunk by clamping to the outer shield and by anchoring to electrical terminals on sapphire insulation plates twice, at the outermost shield and the FE-head. In addition, very thin Teflon-coated wire (Junkosha Inc.; 0.35 mm) was used for all electrical connections in order to suppress thermal conduction.

This system was designed to have several kinds of operation mode; STM, FEM and PM modes. In STM mode, the anode surface is scanned to search for a nanometer-scale hole. In FEM mode, the tip is retracted over the hole, the feedback is turned off, and a negative bias voltage is applied between the tip and hole. The extremely small distance between them induces electric field high enough to extract electrons from the tip. To facilitate STM and FEM modes, a new isolation pre-amplifier has been designed. The amplifier enables the application of high voltage to the tip and anode and the control of the piezotube simultaneously. As shown in Fig. 2, the extracted electron beam is then collimated by the condenser lens inside the anode holder and passes through the holes in the radiation shields for further utilizations; observation of FEM beam pattern on the microchannel plate (MCP), measurement of energy spectra, and observation of interference patterns produced by the beam. The opening angle of an e-beam from conventional tungsten tips is usually so wide that the MCP shows only a small portion of the beam without collimation. In PM mode, an extraction voltage is applied to the tip and the anode is grounded. As the tip approaches the anode object, the extraction voltage is adjusted, usually reduced, in order to maintain the emission current in suitable range (~1 nA). A resistance meter (Advantest, R8340) is employed to measure the emission current as well as to apply negative extraction voltage to the tip.

D. Performance of cooling system.

Once the temperature of the FE-head reaches about 5 K, experiments can run continuously for more than 15 hours before having to stop to transfer additional liquid helium (LHe). The helium tanks are pre-cooled using liquid nitrogen before transferring LHe. For temperature measurement, two silicon diode sensors (Lake Shore, DT-470-SD) are mounted on the FE-head (sensor A, B). Sensor C and D are mounted on the inner and middle radiation shields, respectively. Figure 4 shows a temperature trace during a LHe cooling. In order to confirm the temperature readings of silicon diode sensors, a niobium wire was loaded into the anode holder (Fig. 5) and its resistance was measured by the four-terminal network method. Figure 5 presents the resistance trace with cooling, where the temperature value is the reading of the silicon diode sensor A at the FE-head. Because the superconducting transition temperature of niobium is 9.25 K, the abrupt fall at ~9.5 K demonstrates the correctness of the temperature reading within ±0.5 K.

As shown in the temperature evolution curves in Fig. 4, the temperature rose by ~0.1 K at the FE-head and by ~0.3 K at the inner radiation shield after filling the central He tank, accompanying the rise of the temperature at the middle radiation shield. The middle radiation shield is connected to the top of the central He tank. So the fall of LHe level in the central tank leads to the increase of the temperature at the middle radiation shield. The temperature rise at the radiation shield 2 then raises the temperature at the inner radiation shield and subsequently that at the FE-head through the thermal equilibrium process by radiation.

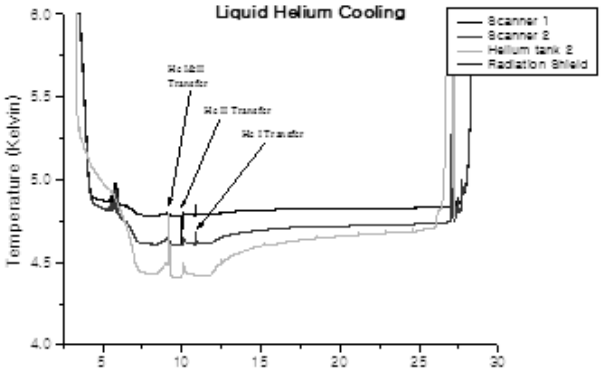

Figure 4. Evolution curve of temperature with LHe cooling.

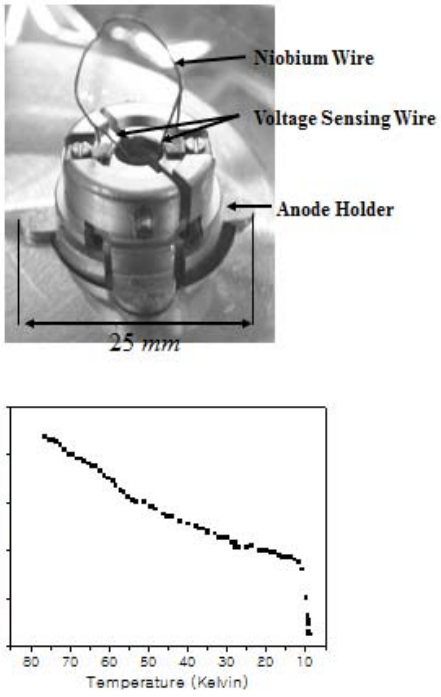

Figure 5. (a) Picture of the experimental setup for measuring the electrical resistance of a Nb wire using the four-terminal network method. The voltage drop across the niobium wire is measured by the voltage sensing wire while flowing constant current through the Nb wire. (b) The evolution of the electrical resistance with LHe cooling.

3. EXPERIMENTAL RESULTS AND DISCUSSION

At the initial stage of tip approach, clear PM images of holy carbon film showed up on the screen, but sometimes rather bright spots appeared near the shadow of carbon film.

The spot images usually turned out to be interference patterns of MWCNT, as shown in Figure 6**.**

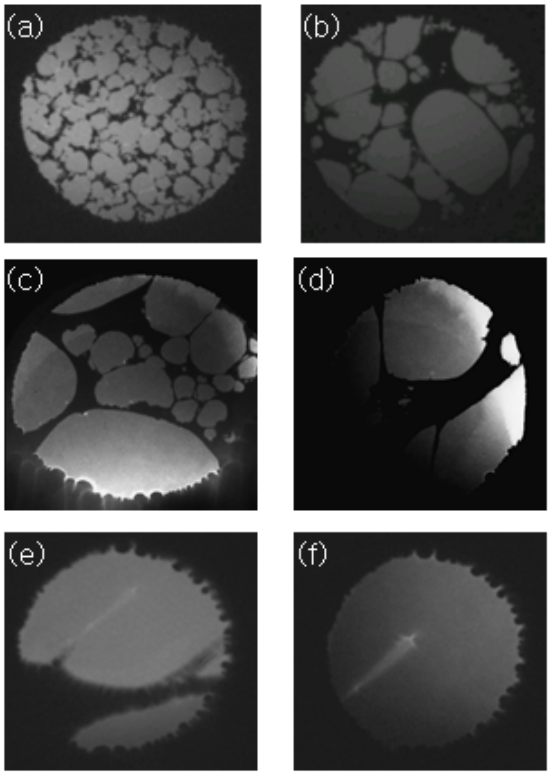

Figure 6. Projection microscopy images of a perforated carbon film and MWCNTs obtained at room temperature.

Figure 7 shows a typical PM images of a MWCNT and the line profile along AB. The line profile gave the average fringe spacing of 0.583 mm with standard deviation of 0.024 mm. The remarkable regularity of fringe spacings in the line profile indicates that the MWCNT would become a biprism. With tip approach the number of fringes increased but the spacing between them remained nearly constant. The width W of the interference region continued to increase and finally became about 2 cm.

In a biprism interferometer, transverse coherence length of an electron source is measured by raising biprism power; i.e. increase of the width of interference region W. The interference region widens with raising biprism voltage for a conventional biprism. When the interference fringes become invisible, the measured W_c corresponds to the transverse coherence length ξ_T of an electron source at the observation plane; W should be smaller than the corresponding coherence length ξ_T of the beam as long as the interference fringe is visible. For the present FE-tip, thus, the transverse coherence length ξ_T should be longer than 2 cm at the screen, quite an impressive value for a normal field emitter. If the field emitter is assumed to be an incoherent source, the effective source size r_{eff} can be calculated by using the van Cittert-Zernike theorem [4]:

$$r_{eff} = \frac{\lambda \cdot l_b}{\pi \cdot \xi_T}$$

Hence ξ_T of > 2 cm gives r_{eff} of < 0.36 nm, which is more than two orders of magnitudes smaller than that of a typical size of field emitter.

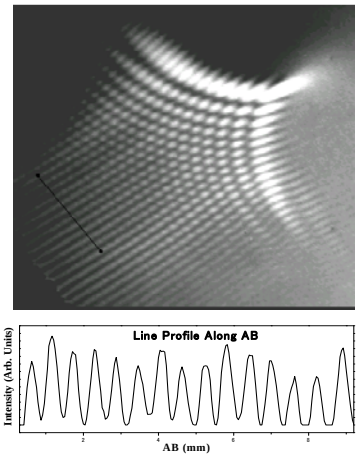

Figure 7 Projection microscopy (PM) mage and a line profile along AB.

The van Cittert-Zernike theorem shows that the transverse coherence length ξ_T would depend on the tip radius and vary from tip to tip [4]. In this experiment, in fact, the ξ_T actually varied with changing tip but slightly in the range of 1.2~2 cm, giving effective source sizes of 0.36~0.7 nm.

Figure 8 shows PM images of another MWCNT with a new FE-tip and the fringe visibility as a function of the width of interference region W. With tip approach and consequent increase of the width of interference region W, the fringe visibility continued to decrease and biprism interference fringes became invisible at $W_c \approx 1.9$ cm, which corresponds to the transverse coherence length ξ_T.

According to the coherence theory, the effective source size is equal to the real size of the source if the source is a fully incoherent one. But effective source sizes obtained from measured transverse coherence length values (0.36~0.7 nm) are too small to be a real size; the FE-emitters may presumably be partially coherent sources. The ratio K of beam radius l_R and transverse coherence length ξ_T was theoretically and experimentally proved to be constant in electron microscopy, by Pozzi et al [10,11]. If a typical value 30 ^{o} is taken for the beam-opening angle, the beam radius on the screen is about 10 cm and the ratio K becomes 0.12 ~ 0.2. Under the assumption that the ratio K is also constant in PM, the coherence length on the surface of the observed field emitter is estimated to be 5 ~ 10 nm for a typical source size value of 50 nm. This finiteness of coherence lengths at the surface of FE emitters is in reasonable agreement with recent observations of FE-patterns from MWCNT [12]. Electrons from different sites of a MWCNT at room temperature, which are a few nm apart, can interfere

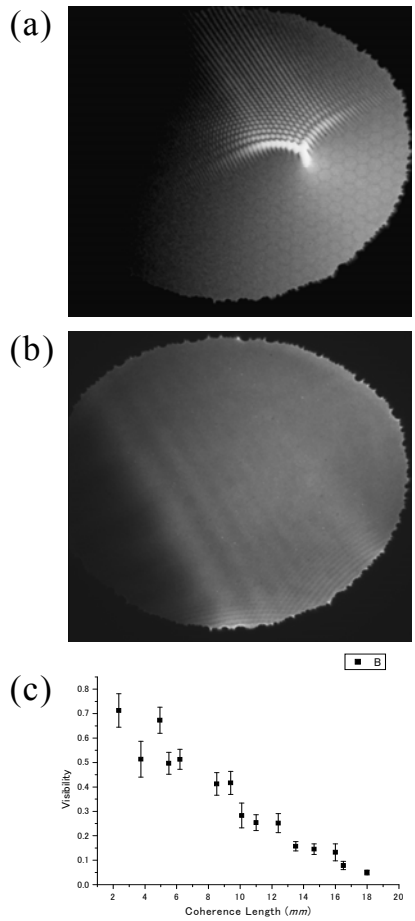

Figure 8. Change of PM image and visibility with tip approach.

with each other on screen, showing that the coherence length on the MWCNT is a few nm.

In solids, in general, the inelastic mean free path of conduction electrons ξ_{in} increases with decreasing temperature because of the reduction of phonon scattering. Hence, interference of electrons traveling along different paths occurs if the path length is shorter than ξ_{in} in solids. The electrical resistivity of tungsten decreases from 5.5 x 10^{-8} to 0.6 x $10^{-8}\Omega$cm in inverse proportion to the temperature in the range from RT to 80K [13]; with such a cooling, ξ_{in} changes from 16nm to 140nm. If the tungsten tip is cooled from RT to low temperature, one can expect a large enhancement of the coherence of the emitted electrons owing to the increase of ξ_{in}. This turned out to be true, as shown below.

Figs. 9(a) and (b) show the interference fringes of electrons emitted from the same tip at RT and 78 K, respectively. They were taken just at the overlapping condition, under which the interference fringes become invisible. The visibility curves V are plotted against the observed width of the interference band. The data points represented by triangles, B1 and circles, B2 at RT in Fig. 10 were obtained by using different nano-biprisms. Both results yielded similar ξ_T values of ~13 *mm* as shown in Fig. 10,

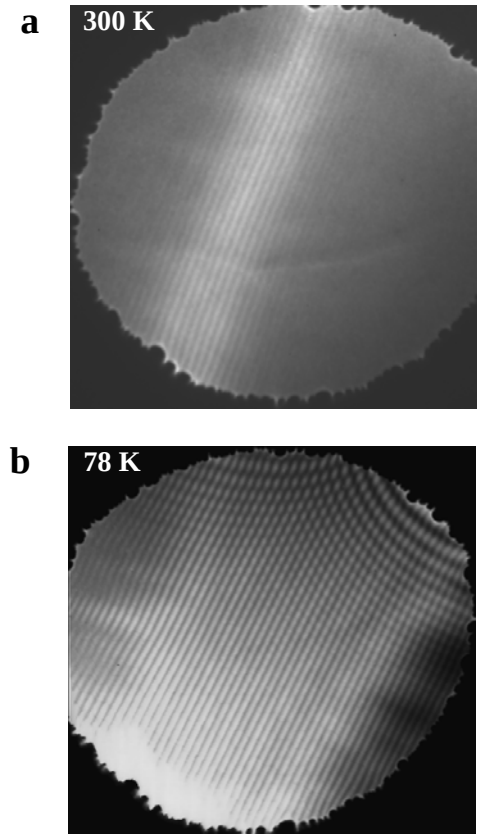

Figure 9. Biprism interference patterns just before the complete blurring of fringes at RT (a), 78 K (b).

which proves that the ξ_T measurement does not depend much on the nano-biprism employed.

As one can see clearly in the patterns of Fig. 9 (a) and (b), the fringes at 78K are much sharper than those at RT, indicating their high visibility. The fringes blurred with the widening of the interference band, but they did not disappear even for values of W above ~70 mm, the maximum diameter of the screen. The ξ_T value at 78 K was longer than ~70 mm, which is more than five times as long as ξ_T at RT (13mm). The coherence length ξ_{in} at the tip was estimated to be 5 ~ 10 nm at RT and ~ 35 nm at 78 K, which are several times or several tens of times as long as the Fermi wavelengths λ_F of the solids. Similar data were also found in STM experiments [14].

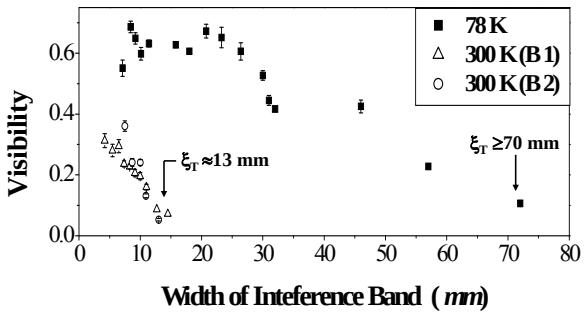

Figure 10. The evolution curves of visibility at RT and at 78 K as a function of the width (W) of interference band.

In summary, the coherence of electrons emitted from tungsten tips at two different temperatures has been evaluated quantitatively. The enhancement of the coherence at 78K agreed quantitatively with the increase in the inelastic mean free path, ξ_{in} in solids calculated on the basis of the conductivity. We are now preparing 5K experiments, under which conditions the inelastic mean free path, ξ_{in} is expected to increase by an additional factor of ~15. These highly coherent electrons will allow developing new technology in many aspects of electron microscopy and electron holography [15], resulting in the creation of new research fields of fundamental physics concerning highly coherent electron beams such as the Aharonove-Bohm effect [15], anti-correlation of electron waves in vacuum [16] and material science & technology.

References

[1] J. C. H. Spence, "Experimental High-Resolution Electron Microscopy", Oxford University Press 1988.

[2] G. F. Missiroli, G. Pozzi and U Valdre, J. Phys. E **14**, 649(1999).

[3] M. Born and E. Wolf, "Principles of Optics", 7th ed., Cambrige University Press.

[4] J .C. H. Spence, W. Qian and M. P. Silverman, J. Vac. Technol. A **12**, 542(1994).

[5] M. J. Fransen, E. P. N. Damen, C. Schiller, T. L. van Rooy, H. B. Groen and P. Kruit, App. Surf. Sci. **94/95**, 107(1996).

[6] N. de Jonge, Y. Lamy, K. Schoots and T. H. Ooseterkamp, Nature **420**, 393(2002).

[7] S. Horiuchi , "Fundamentals of high-resolution transmission electron microscopy", Amsterdam : North-Holland, 1994.

[8] M. Prigent and P. Morin, J. Microscopy **199**, 197(2000).

[9] B. Cho, T. Ogawa, T. Ichimura, T. Ichinokawa and C. Oshima, to be published.

[10] G. Pozzi, Optik **77**, 69(1987).

[11] G. Pozzi, G. Matteucci and R. W. Carpenter, Eleventh International Congress on Electron Microscopy, Kyoto vol 1, 315(1984).

[12] C. Oshima, K. Mastuda, T. Kona, Y. Mogami, M. Komaki, Y. Murata, M. Yamashita, T. Kuzumaki and Y. Horiike, Phys. Rev. Lett. **88**, 38301 (2002).

[13] Meaden, G.. T. Electrical Resistance of Metals. (Heywood Books, London, 1966).

[14] O. Jeandupeux, L. Bu¨rgi, A. Hirstein, H. Brune and K. Kern, Phys. Rev. B **59**, 15926 (1999).

[15]A. Tonomura, Rev. Mod. Phys. **59**, 639(1987).

[16] H. Kiesel, A. Renz., and F. Hasselbach, Nature **418**, 392-394 (2002).